ACS MATERIALS LETTERS

www.acsmaterialsletters.org

LETTER

Novel Class of Proton Conducting Materials—High Entropy Oxides

Maria Gazda,* Tadeusz Miruszewski, Daniel Jaworski, Aleksandra Mielewczyk-Gryń, Wojciech Skubida, Sebastian Wachowski, Piotr Winiarz, Kacper Dzierzgowski, Marcin Łapiński, Iga Szpunar, and Ewa Dzik

Cite This: *ACS Materials Lett.* 2020, 2, 1315–1321

Read Online

ACCESS | Metrics & More | Article Recommendations | Supporting Information

ABSTRACT: **Here, for the first time, we present data on proton conductivity of high-entropy, single-phase perovskites. The $BaZr_{0.2}Sn_{0.2}Ti_{0.2}Hf_{0.2}Ce_{0.2}O_{3-\delta}$, $BaZr_{0.2}Sn_{0.2}Ti_{0.2}Hf_{0.2}Y_{0.2}O_{3-\delta}$, $BaZr_{1/7}Sn_{1/7}Ti_{1/7}Hf_{1/7}Ce_{1/7}Nb_{1/7}Y_{1/7}O_{3-\delta}$, and $BaZr_{0.15}Sn_{0.15}Ti_{0.15}Hf_{0.15}Ce_{0.15}Nb_{0.15}Y_{0.10}O_{3-\delta}$ single-phase perovskites were synthesized. Before electrical measurements, materials were characterized using X-ray diffraction (XRD), scanning electron microscopy (SEM), X-ray photoelectron spectroscopy (XPS), and thermogravimetric analysis (TGA). The following experimental results demonstrated that studied high-entropy perovskites are proton conductors: (1) The observed mass increase upon the switch from dry to wet atmosphere confirmed the water incorporation into materials structure. (2) The electrochemical impedance spectroscopy (EIS) revealed that the total conductivity increased while its activation energy decreased in the presence of water vapor in the atmosphere. (3) The conductivity in atmosphere humidified with H_2O and D_2O differed one from another, showing typical of proton conductors isotope effect in high-entropy oxides.**

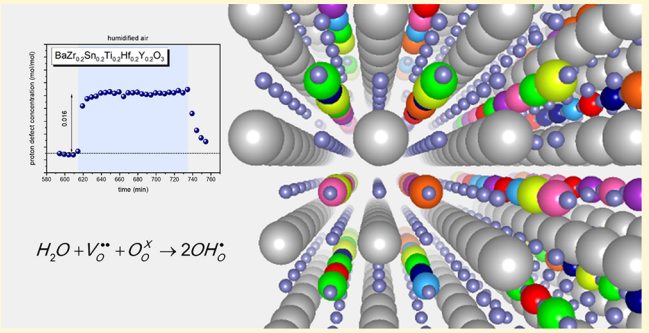

Oxides containing cations introduced to the host structure as substitutions have always been studied; however, the research on high-entropy oxides (HEOs), in which entropy forces the cations in the random distribution, commenced in 2015 from the pioneering work of Rost et al.,[1] who demonstrated that configurational disorder can, at a particular temperature, promote the formation of a homogeneous oxide. Studies on $Mg_{0.2}Co_{0.2}Ni_{0.2}Cu_{0.2}Zn_{0.2}O$ by Bérardan et al. showed constituents may have different valency.[2] What is interesting, the ionic conductivity observed in lithium-substituted high-entropy oxides was very high, reaching 1 mS·cm^{-1} at room temperature.[3] Apart from the HEOs of the rock-salt structure also perovskite,[4−6] fluorite,[7,8] and spinel[9] oxides were studied, as well as multiple other systems.[10,11] Sharma et al. showed that epitaxial films of high-entropy $BaZr_{0.2}Sn_{0.2}Ti_{0.2}Hf_{0.2}Nb_{0.2}O_3$ perovskite deposited on $SrTiO_3$ and MgO exhibited thermal conductivity almost an order of magnitude lower than other, non-HEO, single-crystal perovskites.[4] Jiang et al. synthesized $BaZr_{0.2}Sn_{0.2}Ti_{0.2}Hf_{0.2}Ce_{0.2}O_3$ and $BaZr_{0.2}Sn_{0.2}Ti_{0.2}Hf_{0.2}Y_{0.2}O_{3-\delta}$ high-entropy perovskites showing that aliovalent substitutions are possible in these compounds.[5]

The idea of using high-entropy oxides as proton conductors is based on the possible influence of configurational entropy and related to that disorder on the possibilities of obtaining high concentration and mobility of proton defects. Moreover, compositional variety of these multi-component oxides should allow for adjusting the electrochemical properties by changing oxide constituents. So far, no reports have been published on proton conduction in high-entropy oxides. Proton conduction in oxides requires the formation of protonic defects, $OH_O^{\bullet}$, where $OH_O^{\bullet}$, in Kröger−Vink notation, signifies OH^{1-} occupying the oxygen site. This process occurs in an atmosphere containing water vapor for compounds in which oxygen vacancies are available. Proton defect concentration depends on the concentration of oxygen vacancies available for hydration and hydration enthalpy. While it may be difficult to achieve more favorable hydration thermodynamics than that for the state-of-art perovskites, we believe the entropy may enable introducing higher content of acceptor-type constituents without defect clustering. Proton mobility is affected by energy barrier height, the entropy of migration and proton trapping energy. Proton transport occurs through Grotthus mechanism involving rotation of the OH bond and proton hopping between oxygen

Received: June 16, 2020
Accepted: September 9, 2020
Published: September 9, 2020

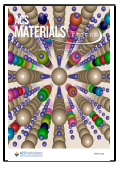

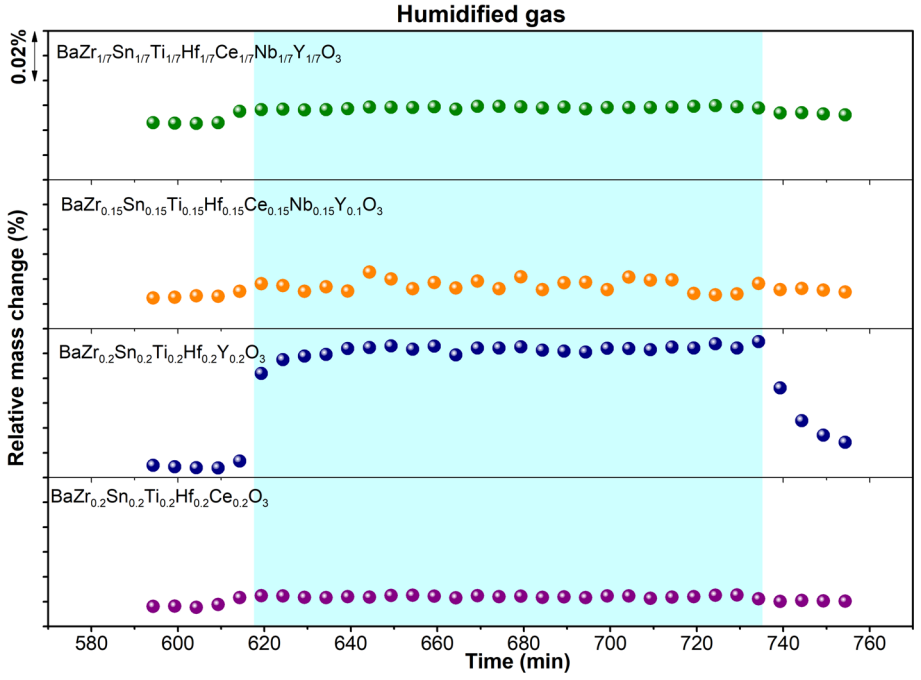

Figure 1. Thermograms recorded at 300 °C upon isothermal switch between dry and humidified atmosphere.

ions.[12] As the first approximation, the oxygen lattice in HEOs may be considered as ordered,[1] however, Bérardan et al.[13] and Rak et al.[14] showed that in rock-salt HEOs Jahn Teller effects introduce some randomness into the oxygen lattice. Similar effects may be present in perovskites. Moreover, cationic lattice disorder causes a distribution in the cation−oxygen bond length and strain. Thus, it may also influence the energy barriers for proton transport, the tendency to defect clustering and proton trapping, which would result in altering the ionic conductivity. Migration entropy, related to the number of possible equivalent proton paths may be influenced by high configurational entropy through introducing frustrated energy landscape relaxing the constraints on jump trajectories. Such a phenomenon was reported in non-HEO Li-ion conductor ($LiTi_2(PS_4)_3$) by Di Stefano et al.[15]

Here, we investigate the possibility of proton conduction in high-entropy cubic perovskites (ABO_3). One set of samples, that is, $BaZr_{0.2}Sn_{0.2}Ti_{0.2}Hf_{0.2}Ce_{0.2}O_{3-\delta}$ and $BaZr_{0.2}Sn_{0.2}Ti_{0.2}Hf_{0.2}Y_{0.2}O_{3-\delta}$, were previously reported as HEOs by Luo et al.[5] The second set, that is, oxides containing seven B-cations ($BaZr_{1/7}Sn_{1/7}Ti_{1/7}Hf_{1/7}Ce_{1/7}Nb_{1/7}Y_{1/7}O_{3-\delta}$ and $BaZr_{0.15}Sn_{0.15}Ti_{0.15}Hf_{0.15}Ce_{0.15}Nb_{0.15}Y_{0.10}O_{3-\delta}$), we report here for the first time. To examine the possible proton conduction, water uptake and electrical conductivity in dry and wet air were studied. For the first time, to our knowledge, proton conductivity has been investigated for high entropy oxides.

All obtained oxides were single-phase cubic perovskites. The results of the structural, microstructural and XPS analyses are given in Supporting Information. The unit cell parameters increase linearly with an increasing average radius of B-cation (Figure S7), which follows the Vegard rule. This may indicate that the oxygen content of the oxides is close to the one resulting from the cation stoichiometry, and the major part of niobium is present as Nb^{5+}. This is supported by the XPS results showing that roughly 90% of Nb in $BaZr_{0.15}Sn_{0.15}Ti_{0.15}Hf_{0.15}Ce_{0.15}Nb_{0.15}Y_{0.1}O_{3-\delta}$ and $BaZr_{1/7}Sn_{1/7}Ti_{1/7}Hf_{1/7}Ce_{1/7}Nb_{1/7}Y_{1/7}O_{3-\delta}$ is present as Nb^{5+} (Figure S9). XPS analysis for other cations (Figures S10−S14) showed that Zr, Sn, Ti, and Hf are at 4+, whereas Y at 3+ valence state. The data for cerium were of too low intensity to determine the Ce^{4+} and Ce^{3+} content. Nevertheless, cerium is known to be stable as Ce^{4+} in $BaCeO_3$-type perovskites at P_{O_2} of $1-10^{-4}$ bar.[16] The microstructures of all samples (Figure S8) are similar, they are porous and consist of well-formed crystalline grains (50−900 nm).

To analyze proton conduction in HEOs, firstly formation of protonic defects should be verified. In good proton-conducting oxides, protonic defects form in the hydration reaction (reaction 1)

$$v_O^{\bullet\bullet} + H_2O_{(g)} + O_O^x = 2OH_O^{\bullet} \quad (1)$$

where $v_o^{\bullet\bullet}$, O_o^x, and $OH_o^{\bullet}$ denote Kröger−Vink symbols of oxygen vacancy, lattice oxygen and protonic defect, respectively.

Thermogravimetric analysis upon isothermal switch at 300°C between the dry ($p_{H_2O} \approx 6 \times 10^{-5}$ atm) and humidified atmosphere ($p_{H_2O} \approx 0.01$ atm, (Figure 1) shows that the relative mass change of $BaZr_{0.2}Sn_{0.2}Ti_{0.2}Hf_{0.2}Y_{0.2}O_{3-\delta}$ is the highest, approximately 0.05%, while for the other samples, it is on the order of 0.005%. The mass change in humid atmosphere can be attributed to hydration as an effect of the proton defects formation. Since the powders were synthesized as bulk—not nanopowders—the surface adsorption is negligible. As shown by reaction 1, oxygen vacancies are necessary for this process. Extrinsic oxygen vacancies in acceptor-doped oxides form to maintain charge neutrality. In the considered HEOs, yttrium and niobium are acceptor- and donor-type constituents, respectively, while the other B-cations (Zr, Sn, Ti, Hf, and Ce) are 4+ ions. Therefore, in $BaZr_{0.2}Sn_{0.2}Ti_{0.2}Hf_{0.2}Ce_{0.2}O_{3-\delta}$ oxygen vacancy concentration is close to zero, or no vacancies are available for hydration, while in $BaZr_{0.2}Sn_{0.2}Ti_{0.2}Hf_{0.2}Y_{0.2}O_{3-\delta}$ one oxygen vacancy per two yttrium ions forms. In $BaZr_{1/7}Sn_{1/7}Ti_{1/7}Hf_{1/7}Ce_{1/7}Nb_{1/7}Y_{1/7}O_{3-\delta}$ with 90% of Nb^{5+}, the average charge of B-cations is slightly lower than 4+, so a small concentration of extrinsic oxygen vacancies may be expected. On the other hand,

https://dx.doi.org/10.1021/acsmaterialslett.0c00257
ACS Materials Lett. 2020, 2, 1315−1321

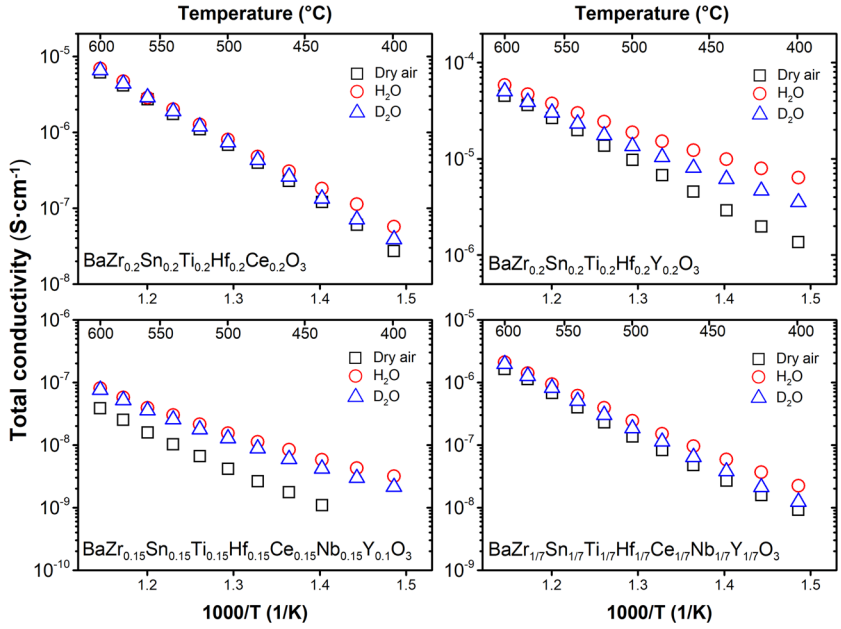

Figure 2. Total electrical conductivity of the HEOs in dry ($p_{O_2} \approx 0.199$ atm, $p_{H_2O} \approx 6 \times 10^{-5}$ atm) and humidified air ($p_{O_2} \approx 0.195$ atm, $p_{H_2O} \approx 2.36 \times 10^{-2}$ atm) with either H_2O or D_2O plotted as a function of inverted temperature.

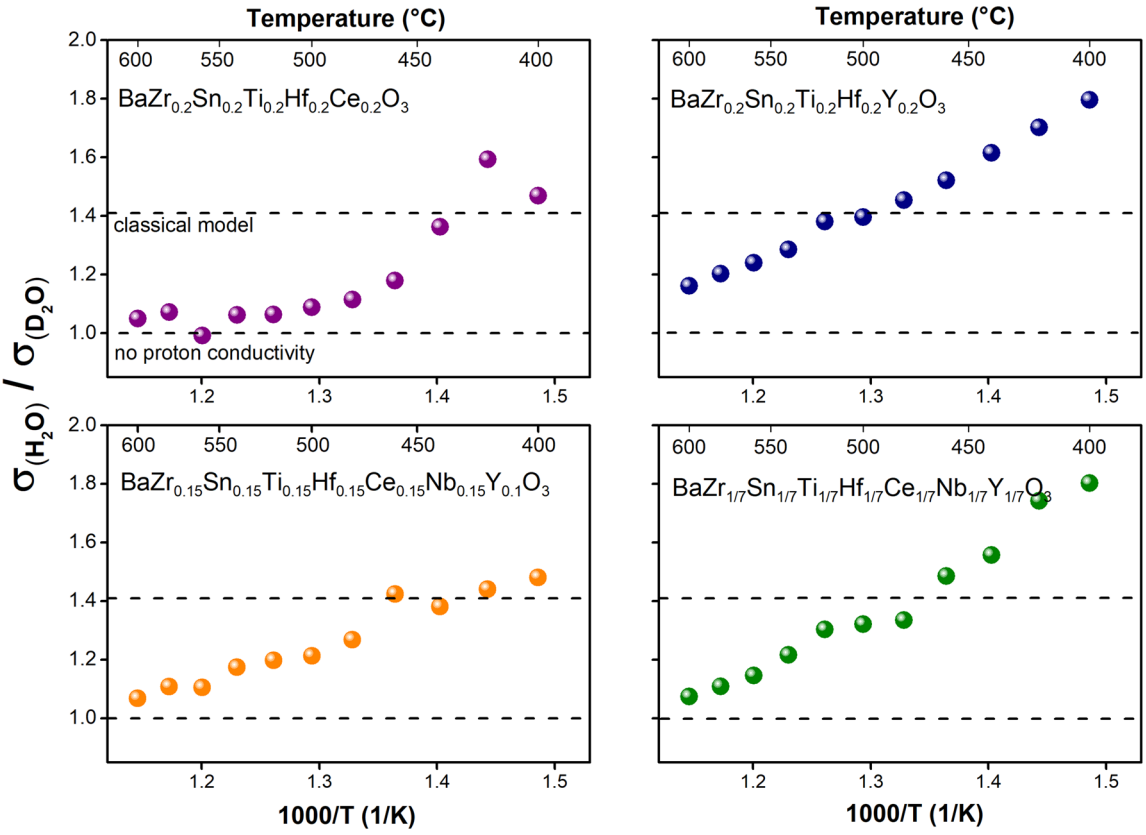

Figure 3. Ratios of total electrical conductivities in H_2O and D_2O-humidified air as a function of inverted temperature. Horizontal lines mark $\sigma_{H_2O}/\sigma_{D_2O}$ equal to $\sqrt{2}$ (classical model of ideal proton conductor) and 1 (non-proton conductor).

in $BaZr_{0.15}Sn_{0.15}Ti_{0.15}Hf_{0.15}Ce_{0.15}Nb_{0.15}Y_{0.1}O_{3-\delta}$, the Nb^{5+} content exceeds that of Y^{3+}; therefore, the charge compensation involving either electronic defects, cation vacancies or oxygen interstitials formation may occur. In barium titanates and stannates various mechanisms of Nb^{5+} charge compensation, involving electronic and ionic processes, were discussed. Singh et al. in $BaSn_{1-x}Nb_xO_3$ proposed that similarly to barium titanate, for $x > 0.010$ B-site vacancies form.[17] Alternatively, barium vacancies formation and reduction of titanium from Ti^{4+} to Ti^{3+} were considered by Jwala et al. in Nb-doped $BaTi_{0.85}Zr_{0.15}O_3$.[18] It should be noted that the presence of barium vacancies increases energy barriers for proton migra-

https://dx.doi.org/10.1021/acsmaterialslett.0c00257
ACS Materials Lett. 2020, 2, 1315−1321

tion.[19] Regardless of which mechanism prevails, the concentration of oxygen vacancies in $BaZr_{0.15}Sn_{0.15}Ti_{0.15}Hf_{0.15}Ce_{0.15}Nb_{0.15}Y_{0.1}O_{3-\delta}$ may be considered very low. Summing up, among the high entropy oxides studied in this work, only $BaZr_{0.2}Sn_{0.2}Ti_{0.2}Hf_{0.2}Y_{0.2}O_{3-\delta}$ contains a significant number of oxygen vacancies, which explains why this sample exhibits the highest water uptake. The relative mass change for this composition corresponds to 1.6×10^{-2} mol/mol proton defect concentration and is similar to other mixed proton−electron conductors like barium lanthanide cobaltites[20] but is lower than in well-recognized proton conducting materials like barium zirconate.[21] Proton defect concentration in $BaZr_{0.2}Sn_{0.2}Ti_{0.2}Hf_{0.2}Ce_{0.2}O_{3-\delta}$, $BaZr_{1/7}Sn_{1/7}Ti_{1/7}Hf_{1/7}Ce_{1/7}Nb_{1/7}Y_{1/7}O_{3-\delta}$, and $BaZr_{0.15}Sn_{0.15}Ti_{0.15}Hf_{0.15}Ce_{0.15}Nb_{0.15}Y_{0.10}O_{3-\delta}$ is 1.5×10^{-3}, 2.0×10^{-3}, and 2.4×10^{-3} mol/mol, respectively. The hydration characteristics of a perovskite oxide depend on such factors as the difference in the electronegativity of the B- and A-cations and the tolerance factor influencing hydration enthalpy.[22] $BaZr_{0.2}Sn_{0.2}Ti_{0.2}Hf_{0.2}Y_{0.2}O_{3-\delta}$ and $BaZr_{0.8}Y_{0.2}O_{3-\delta}$ have similar tolerance factors, but the difference of weighted electronegativity[23] for the B and A constituents ($\chi_B - \chi_A$) is different. Taking the values of Allred−Rochow electronegativities of 0.97, 1.22, 1.72, 1.32, 1.23, and 1.11 for Ba, Zr, Sn, Ti, Hf, and Y, respectively[24] ($\chi_B - \chi_A$) of $BaZr_{0.2}Sn_{0.2}Ti_{0.2}Hf_{0.2}Y_{0.2}O_{3-\delta}$ is 0.35, while that of $BaZr_{0.8}Y_{0.2}O_{3-\delta}$ is 0.228. Norby et al.[22] suggested the larger difference between the electronegativities the less exothermic hydration process. The value observed for $BaZr_{0.2}Sn_{0.2}Ti_{0.2}Hf_{0.2}Y_{0.2}O_{3-\delta}$ is less favorable for hydration than that for $BaZr_{0.8}Y_{0.2}O_{3-\delta}$; however, it corresponds to a negative enthalpy of hydration.[22]

The transport properties of oxides involve electronic and ionic charge carriers. Here, we expect that mobile ionic defects are protonic defects, $OH_o^{\bullet}$, and oxygen vacancies, $v_o^{\bullet\bullet}$. The mobile electronic carriers may be also present. The disorder and lattice distortions, related to the presence of at least five cationic constituents, may influence both the concentration and mobility of charge carriers. The total electrical conductivity of high entropy perovskites in different conditions is displayed in Figures 2 and 3. Apparent activation energies and values of total conductivity at 440 °C are gathered in Table S2.

The total conductivity of the HEOs containing five elements on B-site is higher than that of the oxides containing seven. Nevertheless, the electrical properties of these oxides show several similar features. Firstly, the total conductivity in humidified air is higher than that in dry air. This is especially evident below 500 °C. Moreover, the isotope effect is observed, that is, the conductivity in the atmosphere containing D_2O is lower than that observed in the air humidified with H_2O. The ratios of total conductivities in H_2O- and D_2O-humidified air at low temperature are between 1.4 and 1.8, while with increasing temperature, they decrease approaching unity between approximately 500 and 600 °C. Both the concentration of proton (deuteron) defects[25,26] and their mobility[27] may depend on the isotopic distribution. The presence of conductivity isotope effect is considered as a confirmation of proton contribution. Moreover, such a large value of ratios of total conductivities in H_2O- and D_2O-humidified air as observed in this work confirm the Grotthuss mechanism of conduction.[28] So that, at lower temperatures, proton conduction dominate the transport properties of the materials. Secondly, the activation energy of total conductivity depends on the atmosphere and the temperature range.

In dry air, the charge carriers contributing to the electrical conductivity are either oxygen ions or electronic-type charge carriers, or both, whereas the protonic defects may be neglected. That is why the activation energy of conductivity in dry air is higher, while the values of conductivity are lower than those observed in humidified air. The values of activation energy of conductivity in dry air are higher than those observed in low-entropy proton-conducting perovskites. For example, Zając et al. reported 1.05 eV for $BaZr_{0.95}Gd_{0.05}O_{2.975}$,[29] and Bohn et al. for $BaZr_{0.9}Y_{0.1}O_{2.95}$ found 0.9 and 1.1 eV and interpreted them as related to electron−hole and oxygen ion conduction, respectively.[30] Assuming small polaron hopping conduction in dry air, the high activation energy of conductivity of HEOs would be justified by enhancing the tendency of electron-hole trapping as small polarons by the lattice disorder.[31] It is not known how B-cation disorder influences the oxygen ion conductivity in perovskites; however, Luo et al., who studied HEOs based on the ZrO_2, observed higher activation energy of oxygen ion conductivity in comparison to that in the low entropy yttria-stabilized zirconia.[8] It should be also noted that the $BaZr_{0.15}Sn_{0.15}Ti_{0.15}Hf_{0.15}Ce_{0.15}Nb_{0.15}Y_{0.1}O_{3-\delta}$ oxide in which neither oxygen vacancies nor electron-hole type charge carriers are expected to significantly contribute to the conductivity in dry air, exhibits the lowest total conductivity.

To discuss the proton conduction, we will first focus on the properties of $BaZr_{0.2}Sn_{0.2}Ti_{0.2}Hf_{0.2}Ce_{0.2}O_{3-\delta}$ and acceptor-substituted $BaZr_{0.2}Sn_{0.2}Ti_{0.2}Hf_{0.2}Y_{0.2}O_{3-\delta}$ in the humidified atmosphere below 500 °C. Acceptor-type substitution is a typical strategy of increasing proton conductivity; therefore, their properties may be compared with those of low entropy perovskites, for example, $BaZrO_3$ and acceptor-substituted $BaZrO_3$.

Similarly to typical proton conductors, $BaZr_{0.2}Sn_{0.2}Ti_{0.2}Hf_{0.2}Y_{0.2}O_{3-\delta}$ in wet air at temperatures below 500 °C uptakes water and exhibits higher total electrical conductivity than in dry air. Interestingly, apparent activation energy of total conductivity of $BaZr_{0.2}Sn_{0.2}Ti_{0.2}Hf_{0.2}Y_{0.2}O_{3-\delta}$ (0.53 eV) in wet atmosphere is lower than that exhibited by low-entropy doped barium zirconate (e.g., 0.73 eV for $BaZr_{0.9}Sc_{0.1}O_3$, 0.54 eV for $BaZr_{0.85}Sc_{0.05}Yb_{0.05}O_3$,[32] 0.62 eV for $BaZr_{0.8}Y_{0.2}O_3$,[33] 0.8−1 eV in $BaZr_{0.8}M_{0.2}O_{3-x}$ for M = Sc, In, Lu, Y, and Sm, and 0.73 eV for M = Gd[34]). Terms that contribute to the activation energy of proton conductivity are energy barriers for proton hopping, hydroxide ion rotation, and proton trapping energy. Moreover, the apparent activation energy of total conductivity is strongly influenced by grain boundary conductivity. The activation energy of proton motion depends on the A-ion characteristics and O−B−O bending.[19] Because of atomic mass difference, phonons related to O−B−O vibrations in $BaZr_{0.2}Sn_{0.2}Ti_{0.2}Hf_{0.2}Y_{0.2}O_{3-\delta}$ should shift towards lower frequencies in comparison with $BaZr_{0.8}Y_{0.2}O_{3-\delta}$. That indicates softening of the energy barrier for the O−B−O deformation. Regarding the proton trapping energy, Gilardi et al. suggested, that in doped barium zirconates it is determined by the dopant-host ionic radii mismatch.[34] In high entropy oxides, the conception of host and dopant is no longer applicable but the ionic radii differences and disorder related to that are most probably also relevant for proton trapping. Finally, in porous $BaZr_{0.2}Sn_{0.2}Ti_{0.2}Hf_{0.2}Y_{0.2}O_{3-\delta}$, grain-boundary conductivity influence on the apparent activation energy of total conductivity cannot be neglected. Since porosity is related to low sinterability, it would indicate a rather high activation energy of grain-boundary conductivity. Thus, observed relatively low apparent activation energy of total

https://dx.doi.org/10.1021/acsmaterialslett.0c00257
ACS Materials Lett. 2020, 2, 1315−1321

conductivity of $BaZr_{0.2}Sn_{0.2}Ti_{0.2}Hf_{0.2}Y_{0.2}O_{3-\delta}$ seems a promising feature of proton transport, meaning that further optimization of the composition and microstructure of these oxides will allow obtaining high proton conductivity.

The total conductivity in humidified air and its activation energy differ depending on whether the air is saturated with H_2O or D_2O. In $BaZr_{0.2}Sn_{0.2}Ti_{0.2}Hf_{0.2}Y_{0.2}O_{3-\delta}$, the $\sigma_{H_2O}/\sigma_{D_2O}$ ratio is 1.8 at 400 °C and decreases with increasing temperature reflecting a decreasing proton/deuteron contribution to the total conductivity. For comparison, in not-containing acceptor-type constituent $BaZr_{0.2}Sn_{0.2}Ti_{0.2}Hf_{0.2}Ce_{0.2}O_{3-\delta}$, the ratio of σ_{H_2O} and σ_{D_2O} at 400 °C is 1.4 and approaches unity at 470 °C confirming that proton conductivity in this material is low. Conductivity isotope effect in proton-conducting oxides may be discussed within a few models. The classical model saying that replacing H with D leads to a decrease of the pre-exponential term of the conductivity by $\sqrt{2}$, with no change in the activation energy[27] may be ruled out since a difference between activation energies of conductivity in air containing H_2O or D_2O is observed. As described by the semi-classical model, a difference in activation energies is caused by different zero-point energies of proton and deuteron in the potential well. This model is more satisfactory, however, in the case of $BaZr_{0.2}Sn_{0.2}Ti_{0.2}Hf_{0.2}Y_{0.2}O_{3-\delta}$, the difference between activation energies ($E_A(D_2O) - E_A(H_2O) = 0.12 \pm 0.04$ eV) exceeds the predicted maximum value of 0.055 eV.[28] Larger than predicted difference in activation energies may result from different trapping energies for H and D or other phenomena influencing the D−O and H−O bonds not included within the semiclassical model.

In summary, on the basis of the described above properties of $BaZr_{0.2}Sn_{0.2}Ti_{0.2}Hf_{0.2}Y_{0.2}O_{3-\delta}$, proton defects formation, conductivity isotope effect, higher conductivity, and relatively low apparent activation energy of conductivity in a humid atmosphere, it may be concluded that this HEO is a promising proton-conducting oxide. Nevertheless, it should be noted that the conductivity level shown by $BaZr_{0.2}Sn_{0.2}Ti_{0.2}Hf_{0.2}Y_{0.2}O_{3-\delta}$ in the humid atmosphere is still significantly lower than that of the state-of-art perovskites, that is, double-[35] or triple-doped[36] solid solutions of barium cerate and zirconate. For example, total conductivity in wet air at 600 °C of dense $BaCe_{0.5}Zr_{0.2}Y_{0.1}Yb_{0.1}Gd_{0.1}O_{3-\delta}$ achieved 1×10^{-2} S cm^{-1}.[36]

Further discussion will be devoted to possible proton conduction in $BaZr_{0.15}Sn_{0.15}Ti_{0.15}Hf_{0.15}Ce_{0.15}Nb_{0.15}Y_{0.1}O_{3-\delta}$ and $BaZr_{1/7}Sn_{1/7}Ti_{1/7}Hf_{1/7}Ce_{1/7}Nb_{1/7}Y_{1/7}O_{3-\delta}$. These oxides form more complex systems because of the higher number of constituents and the presence of niobium. As discussed before, the concentration of extrinsic oxygen vacancies in $BaZr_{1/7}Sn_{1/7}Ti_{1/7}Hf_{1/7}Ce_{1/7}Nb_{1/7}Y_{1/7}O_{3-\delta}$ is small but higher than that in the other virtually nonhydrating compositions. Despite that, in both oxides the mass gains upon exposition to water are similar. On the other hand, the isotope effect values and temperature dependencies in both oxides differ. The ratio of σ_{H_2O} and σ_{D_2O} at 400 °C (Figure 2) in $BaZr_{1/7}Sn_{1/7}Ti_{1/7}Hf_{1/7}Ce_{1/7}Nb_{1/7}Y_{1/7}O_{3-\delta}$ is 1.8 and decreases with the increasing temperature reaching unity above 550 °C. This behavior is similar to that observed for $BaZr_{0.2}Sn_{0.2}Ti_{0.2}Hf_{0.2}Y_{0.2}O_{3-\delta}$. In $BaZr_{0.15}Sn_{0.15}Ti_{0.15}Hf_{0.15}Ce_{0.15}Nb_{0.15}Y_{0.1}O_{3-\delta}$, similarly to $BaZr_{0.2}Sn_{0.2}Ti_{0.2}Hf_{0.2}Ce_{0.2}O_{3-\delta}$, σ_H/σ_D at 400 °C is 1.4 and reaches unity below 500 °C. This suggests that proton conduction occurs but that its contribution to the total one in $BaZr_{0.15}Sn_{0.15}Ti_{0.15}Hf_{0.15}Ce_{0.15}Nb_{0.15}Y_{0.1}O_{3-\delta}$ is smaller than in $BaZr_{1/7}Sn_{1/7}Ti_{1/7}Hf_{1/7}Ce_{1/7}Nb_{1/7}Y_{1/7}O_{3-\delta}$. What is surprising and seems to contradict the above statement is the strong influence of the humidity on the total conductivity of $BaZr_{0.15}Sn_{0.15}Ti_{0.15}Hf_{0.15}Ce_{0.15}Nb_{0.15}Y_{0.1}O_{3-\delta}$. The total conductivity at 440 °C increases approximately 5 times, whereas the activation energy of conductivity upon introducing H_2O into the atmosphere becomes relatively low (0.78 eV). It should be noted that the activation energy of conductivity of $BaZr_{1/7}Sn_{1/7}Ti_{1/7}Hf_{1/7}Ce_{1/7}Nb_{1/7}Y_{1/7}O_{3-\delta}$ in the same conditions is much higher (1.10 eV). In summary, the 7-component oxides, because of the presence of niobium, present low total and proton conductivity; however, their electrical properties are interesting and require further research.

In conclusion, we report the properties of proton-conducting high entropy perovskites. All studied oxides formed cubic perovskites with unit cell parameters related to the average B-cation radii following the Vegard rule. We confirmed that high entropy oxides based on barium zirconate exhibit proton conductivity. In all studied oxides, the formation of protonic defects was observed. Moreover, the conductivity in the humidified atmosphere was higher than in dry air, as well as showing results typical of proton conductors isotope effect. $BaZr_{0.2}Sn_{0.2}Ti_{0.2}Hf_{0.2}Y_{0.2}O_{3-\delta}$, which exhibited significant mass gain and high total conductivity in a humid atmosphere, because of the relatively low apparent activation energy of conductivity in a humid atmosphere, was considered as the most promising proton-conducting HEO. The compositional disorder, that is, the presence of five constituents did not cause an increase of activation energy of conductivity. We believe that further optimization of the composition and microstructure of these oxides will allow obtaining high proton conductivity.

EXPERIMENTAL METHODS

The oxides were synthesized with solid-state reaction. Their structural and microstructural properties were analyzed with X-ray diffraction (XRD) and scanning electron microscopy (SEM), respectively. $BaZr_{1/7}Sn_{1/7}Ti_{1/7}Hf_{1/7}Ce_{1/7}Nb_{1/7}Y_{1/7}O_{3-\delta}$ and $BaZr_{0.15}Sn_{0.15}Ti_{0.15}Hf_{0.15}Ce_{0.15}Nb_{0.15}Y_{0.1}O_{3-\delta}$ were analyzed with X-ray photoelectron spectroscopy (XPS). The water uptake was studied using thermogravimetric analysis. Electrical properties were investigated by impedance spectroscopy in dry- and in H_2O- and D_2O-humidified air. All experimental procedures are described in detail in the Supporting Information.

ASSOCIATED CONTENT

Supporting Information

The Supporting Information is available free of charge at https://pubs.acs.org/doi/10.1021/acsmaterialslett.0c00257.

Details of experimental procedures, experimental section on the samples synthesis, results of XRD, SEM, and XPS analysis, Rietveld analysis of the XRD patterns, crystallographic data obtained from the analysis, discussion of the microstructural properties, discussion of the XPS results, and a table gathering electrical properties of the studied HEOs (PDF)

AUTHOR INFORMATION

Corresponding Author

Maria Gazda − *Faculty of Applied Physics and Mathematics and Advanced Materials Centre, Gdańsk University of Technology, 80-233 Gdańsk, Poland;* orcid.org/0000-0001-6193-7815; Email: maria.gazda@pg.edu.pl

https://dx.doi.org/10.1021/acsmaterialslett.0c00257
ACS Materials Lett. 2020, 2, 1315−1321

Authors

Tadeusz Miruszewski − *Faculty of Applied Physics and Mathematics and Advanced Materials Centre, Gdańsk University of Technology, 80-233 Gdańsk, Poland*

Daniel Jaworski − *Faculty of Applied Physics and Mathematics and Advanced Materials Centre, Gdańsk University of Technology, 80-233 Gdańsk, Poland;* orcid.org/0000-0001-5791-6413

Aleksandra Mielewczyk-Gryń − *Faculty of Applied Physics and Mathematics and Advanced Materials Centre, Gdańsk University of Technology, 80-233 Gdańsk, Poland;* orcid.org/0000-0001-6795-3840

Wojciech Skubida − *Faculty of Applied Physics and Mathematics and Advanced Materials Centre, Gdańsk University of Technology, 80-233 Gdańsk, Poland*

Sebastian Wachowski − *Faculty of Applied Physics and Mathematics and Advanced Materials Centre, Gdańsk University of Technology, 80-233 Gdańsk, Poland;* orcid.org/0000-0003-3752-0432

Piotr Winiarz − *Faculty of Applied Physics and Mathematics and Advanced Materials Centre, Gdańsk University of Technology, 80-233 Gdańsk, Poland*

Kacper Dzierzgowski − *Faculty of Applied Physics and Mathematics and Advanced Materials Centre, Gdańsk University of Technology, 80-233 Gdańsk, Poland*

Marcin Łapiński − *Faculty of Applied Physics and Mathematics and Advanced Materials Centre, Gdańsk University of Technology, 80-233 Gdańsk, Poland*

Iga Szpunar − *Faculty of Applied Physics and Mathematics and Advanced Materials Centre, Gdańsk University of Technology, 80-233 Gdańsk, Poland*

Ewa Dzik − *Faculty of Applied Physics and Mathematics and Advanced Materials Centre, Gdańsk University of Technology, 80-233 Gdańsk, Poland*

Complete contact information is available at: https://pubs.acs.org/10.1021/acsmaterialslett.0c00257

Notes

The authors declare no competing financial interest.

■ ACKNOWLEDGMENTS

The research was partially financially supported by the National Science Centre (NCN), Poland, within the projects 2019/35/B/ST5/00888 and 2016/23/B/ST5/02137.

■ REFERENCES

(1) Rost, C. M.; Sachet, E.; Borman, T.; Moballegh, A.; Dickey, E. C.; Hou, D.; Jones, J. L.; Curtarolo, S.; Maria, J. P. Entropy-Stabilized Oxides. *Nat. Commun.* **2015**, *6*, 8485.

(2) Bérardan, D.; Franger, S.; Dragoe, D.; Meena, A. K.; Dragoe, N. Colossal Dielectric Constant in High Entropy Oxides. *Phys. Status Solidi RRL* **2016**, *10*, 328−333.

(3) Bérardan, D.; Franger, S.; Meena, A. K.; Dragoe, N. Room Temperature Lithium Superionic Conductivity in High Entropy Oxides. *J. Mater. Chem. A* **2016**, *4*, 9536−9541.

(4) Sharma, Y.; Musico, B. L.; Gao, X.; Hua, C.; May, A. F.; Herklotz, A.; Rastogi, A.; Mandrus, D.; Yan, J.; Lee, H. N.; Chisholm, M. F.; Keppens, V.; Ward, T. Z. Single-Crystal High Entropy Perovskite Oxide Epitaxial Films. *Phys. Rev. Mater.* **2018**, *2*, 060404.

(5) Jiang, S.; Hu, T.; Gild, J.; Zhou, N.; Nie, J.; Qin, M.; Harrington, T.; Vecchio, K.; Luo, J. A New Class of High-Entropy Perovskite Oxides. *Scr. Mater.* **2018**, *142*, 116−120.

(6) Sarkar, A.; Djenadic, R.; Wang, D.; Hein, C.; Kautenburger, R.; Clemens, O.; Hahn, H. Rare Earth and Transition Metal Based Entropy Stabilised Perovskite Type Oxides. *J. Eur. Ceram. Soc.* **2018**, *38*, 2318−2327.

(7) Chen, K.; Pei, X.; Tang, L.; Cheng, H.; Li, Z.; Li, C.; Zhang, X.; An, L. A Five-Component Entropy-Stabilized Fluorite Oxide. *J. Eur. Ceram. Soc.* **2018**, *38*, 4161−4164.

(8) Gild, J.; Samiee, M.; Braun, J. L.; Harrington, T.; Vega, H.; Hopkins, P. E.; Vecchio, K.; Luo, J. High-Entropy Fluorite Oxides. *J. Eur. Ceram. Soc.* **2018**, *38*, 3578−3584.

(9) Dąbrowa, J.; Stygar, M.; Mikuła, A.; Knapik, A.; Mroczka, K.; Tejchman, W.; Danielewski, M.; Martin, M. Synthesis and Microstructure of the (Co, Cr, Fe, Mn, Ni)$_3$O$_4$ High Entropy Oxide Characterized by Spinel Structure. *Mater. Lett.* **2018**, *216*, 32−36.

(10) Tseng, K. P.; Yang, Q.; McCormack, S. J.; Kriven, W. M. High-Entropy, Phase-Constrained, Lanthanide Sesquioxide. *J. Am. Ceram. Soc.* **2020**, *103*, 569−576.

(11) Teng, Z.; Zhu, L.; Tan, Y.; Zeng, S.; Xia, Y.; Wang, Y.; Zhang, H. Synthesis and Structures of High-Entropy Pyrochlore Oxides. *J. Eur. Ceram. Soc.* **2020**, *40*, 1639−1643.

(12) Kreuer, K. D. On the Complexity of Proton Conduction Phenomena. *Solid State Ionics* **2000**, *137*, 149.

(13) Berardan, D.; Meena, A. K.; Franger, S.; Herrero, C.; Dragoe, N. Controlled Jahn-Teller Distortion in (MgCoNiCuZn)O-Based High Entropy Oxides. *J. Alloys Compd.* **2017**, *704*, 693−700.

(14) Rák, Z.; Maria, J. P.; Brenner, D. W. Evidence for Jahn-Teller Compression in the (Mg Co Ni Cu Zn)O Entropy-Stabilized Oxide: A DFT Study. *Mater. Lett.* **2018**, *217*, 300−303.

(15) Di Stefano, D.; Miglio, A.; Robeyns, K.; Filinchuk, Y.; Lechartier, M.; Senyshyn, A.; Ishida, H.; Spannenberger, S.; Prutsch, D.; Lunghammer, S.; Rettenwander, D.; Wilkening, M.; Roling, B.; Kato, Y.; Hautier, G. Superionic Diffusion through Frustrated Energy Landscape. *Chem.* **2019**, *5*, 2450−2460.

(16) Oishi, M.; Yashiro, K.; Sato, K.; Mizusaki, J.; Kitamura, N.; Amezawa, K.; Kawada, T.; Uchimoto, Y. Oxygen Nonstoichiometry of the Perovskite-Type Oxides $BaCe_{0.9}M_{0.1}O_{3-\delta}$ (M-Y, Yb, Sm, Tb, and Nd). *Solid State Ionics* **2008**, *179*, 529−535.

(17) Singh, P.; Sebastian, C. P.; Kumar, D.; Parkash, O. Correlation of Microstructure and Electrical Conduction Behaviour with Defect Structure of Niobium Doped Barium Stannate. *J. Alloys Compd.* **2007**, *437*, 34−38.

(18) Jwala, J. P.; Subohi, O.; Malik, M. M. Influence of B-Site Modification by Hetrovalent (Nb5+) and Isovalent (Zr4+) Dopants in $BaTiO_3$ on Its Dielectric and Electrical Properties Synthesized by Novel Sol Gel Route. *Mater. Res. Express* **2019**, *6*, 096308.

(19) Jing, Y.; Aluru, N. R. The Role of A-Site Ion on Proton Diffusion in Perovskite Oxides (ABO_3). *J. Power Sources* **2020**, *445*, 227327.

(20) Strandbakke, R.; Cherepanov, V. A.; Zuev, A. Y.; Tsvetkov, D. S.; Argirusis, C.; Sourkouni, G.; Prünte, S.; Norby, T. Gd- and Pr-Based Double Perovskite Cobaltites as Oxygen Electrodes for Proton Ceramic Fuel Cells and Electrolyser Cells. *Solid State Ionics* **2015**, *278*, 120−132.

(21) Gonçalves, M. D.; Mielewczyk-Gryń, A.; Maram, P. S.; Kryścio, Ł.; Gazda, M.; Navrotsky, A. Systematic Water Uptake Energetics of Yttrium-Doped Barium Zirconate—A High Resolution Thermochemical Study. *J. Phys. Chem. C* **2020**, *124*, 11308−11316.

(22) Norby, T.; Widerøe, M.; Glöckner, R.; Larring, Y. Hydrogen in Oxides. *Dalt. Trans.* **2004**, 3012−3018.

(23) Allred, A. L.; Rochow, E. G. A Scale of Electronegativity Based on Electrostatic Force. *J. Inorg. Nucl. Chem.* **1958**, *5*, 264−268.

(24) Little, E. J.; Jones, M. M. A Complete Table of Electronegativities. *J. Chem. Educ.* **1960**, *37*, 231−233.

(25) Tsidilkovski, V. I. Thermodynamic Isotope Effect H/D/T in Proton-Conducting Oxides. *Solid State Ionics* **2003**, *162-163*, 47−53.

(26) Bonanos, N.; Huijser, A.; Poulsen, F. W. H/D Isotope Effects in High Temperature Proton Conductors. *Solid State Ionics* **2015**, *275*, 9−13.

(27) Bonanos, N. Oxide-Based Protonic Conductors: Point Defects and Transport Properties. *Solid State Ionics* **2001**, *145*, 265−274.

(28) Nowick, A. S.; Vaysleyb, A. V. Isotope Effect and Proton Hopping in High-Temperature Protonic Conductors. *Solid State Ionics* **1997**, *97*, 17−26.

(29) Zając, W.; Rusinek, D.; Zheng, K.; Molenda, J. Applicability of Gd-Doped $BaZrO_3$, $SrZrO_3$, $BaCeO_3$ and $SrCeO_3$ Proton Conducting Perovskites as Electrolytes for Solid Oxide Fuel Cells. *Cent. Eur. J. Chem.* **2013**, *11*, 471−484.
(30) Bohn, H. G.; Schober, T. Electrical Conductivity of the High-Temperature Proton Conductor $BaZr_{0.9}Y_{0.1}O_{2.95}$. *J. Am. Ceram. Soc.* **2000**, *83*, 768−772.
(31) Emin, D. Small-Polaron Formation. *Phys. Rev. B* **1994**, *49*, 290−300.
(32) Satapathy, A.; Sinha, E.; Rout, S. K. Investigation of Proton Conductivity in Sc and Yb Co-Doped Barium Zirconate Ceramics. *Mater. Res. Express* **2019**, *6*, 056305.
(33) Fabbri, E.; Pergolesi, D.; Licoccia, S.; Traversa, E. Does the Increase in Y-Dopant Concentration Improve the Proton Conductivity of $BaZr_{1-X}Y_xO_{3-\delta}$ Fuel Cell Electrolytes? *Solid State Ionics* **2010**, *181*, 1043−1051.
(34) Gilardi, E.; Fabbri, E.; Bi, L.; Rupp, J. L. M.; Lippert, T.; Pergolesi, D.; Traversa, E. Effect of Dopant-Host Ionic Radii Mismatch on Acceptor-Doped Barium Zirconate Microstructure and Proton Conductivity. *J. Phys. Chem. C* **2017**, *121*, 9739−9747.
(35) Duan, C.; Huang, J.; Sullivan, N.; O'Hayre, R. Proton-Conducting Oxides for Energy Conversion and Storage. *Appl. Phys. Rev.* **2020**, *7*, 011314.
(36) Rajendran, S.; Thangavel, N. K.; Ding, H.; Ding, Y.; Ding, D.; Reddy Arava, L. M. Tri-Doped $BaCeO_3$-$BaZrO_3$ as a Chemically Stable Electrolyte with High Proton-Conductivity for Intermediate Temperature Solid Oxide Electrolysis Cells (SOECs). *ACS Appl. Mater. Interfaces* **2020**, *12*, 38275−38284.

https://dx.doi.org/10.1021/acsmaterialslett.0c00257
ACS Materials Lett. 2020, 2, 1315−1321